IJCRT.ORG ISSN : 2320-2882

INTERNATIONAL JOURNAL OF CREATIVE RESEARCH THOUGHTS (IJCRT)

An International Open Access, Peer-reviewed, Refereed Journal

Prophetical Artificial Intelligence Programme On Thin Film Evaporation In Sequence Formation

Dr. Gayaan Singh[1], Dr.Vinay Dua[2], Shishir Dua[3]

Assistant Professor,Dept.of Physics G.M.V.College,Rampur Maniharan Saharanpur

Assistant Professor & Head, Dept.of Physics R.S.M.(P.G)College,Dhampur (Bijnor)

Scholar

ABSTRACT:-. The trend in miniaturization and enhanced functional performance of integrated circuits and power electronics and photonics has amplified the generated thermal energy in these devices making thermal management a bottleneck for further advancement in these fields. A range of geometries of Sequence structures are developed and examined to address this challenge. However, the numerous form factors and dimension of hierarchical structures in addition to cost and time-consuming synthesis and test procedures make it unfeasible to explore bountiful variations of hierarchical geometries through experimental methods. Here, we introduce a general Artificial Intelligence (AI) platform to address this challenge and guide discovery of hierarchical structures for extreme thermal management of high-performance 2 photonics/electronics. The AI platform is based on Random Forest (RF) algorithm, a robust AI method, and was trained using a large collected experimental data set corresponding to thin film evaporation in various forms of Sequence structures. Four geometrical dimensions of the hierarchical structures and two dimensionless numbers governing heat transfer and fluid dynamics in these structures were used as independent variables to predict heat flux in these structures. The trained model's performance was analyzed using statistical metrics and showed an excellent prediction of heat flux for all the structures with various working fluids. The performance of predictive AI platform was further validated by two independent studies of different research groups. This predictive platform provides a foundation for rational discovery of Sequence structures and working fluids to address the ongoing challenge of thermal management in broad spectrum of technologies including electronics, hypersonic aviation and electric vehicles.

KEYWORDS. Thermal management, Evaporation, Sequence structures, AI.

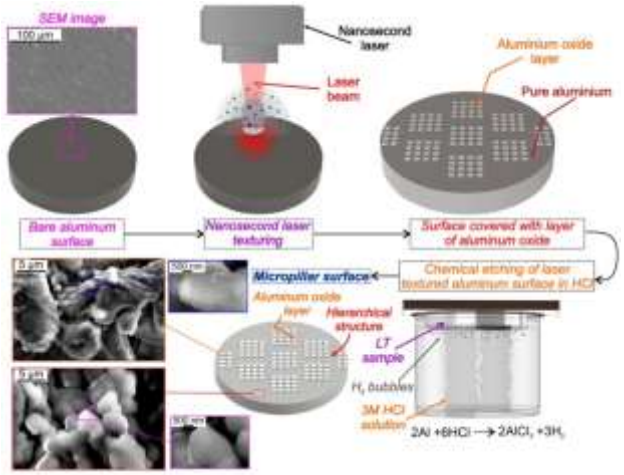

INTRODUCTION Advancements in high-performance photonics/electronics devices have been exponential during the last few decades. Miniaturization along with consistent performance boost in transistors, chips, smartphone, vehicle electronics and server farms has led to high power density and introduced a high demand for advanced cooling techniques1. A range of methods has been studied to address the thermal management challenge, including microchannels[2,3], sprays[4], and jet impingement[5] . However, thin film evaporation have received special interests owing to the potential to dissipate high heat fluxes. Over the last two decades, extensive experimental studies have been conducted on thin film evaporation in hierarchical structures including micro and nano pillar arrays, nano-membranes, copper micro-posts, multi-artery, and sintered wick micro/nanostructures. Despite a large body of experimental works, the path for a three accurate and robust model that predicts heat flux corresponding to thin film evaporation in various form factor of hierarchical structures remains elusive. Fabrication of hierarchical structures and experimental measurements of thin film evaporation performance are costly and time-consuming. In addition, variations in the form factor and dimension of hierarchical structures is so broad making it unfeasible to explore these variations through experimental efforts. A credible alternative to minimize and complement

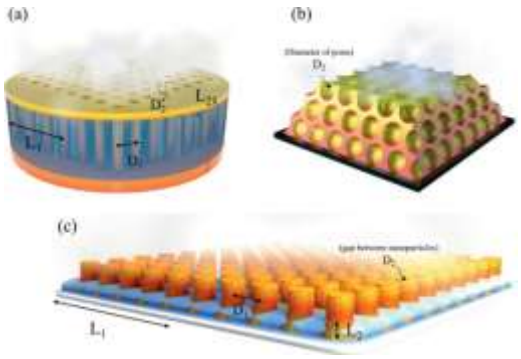

Figure 1

the fabrication and experimental challenges is to capture an unsolved relationship between heat flux vs geometrical and physical variables via data science. Recently, the field of nanoscience and engineering has been exploring Artificial Intelligence (AI) to avoid high-cost and time consuming experimental works. Here, we present an integrated AI-enabled predictive model for thin film evaporation in hierarchical structures. We take advantage of physics of thin film evaporation, data extracted from literature and use Random Forest (RF), a robust AI method, to train and validate a general AI model. The developed model predicts heat flux in hierarchical structures for various working fluids as a function of geometrical dimensions and two dimensionless numbers. The first dimensionless number (Ja: Jacob number) governs heat transfer in the

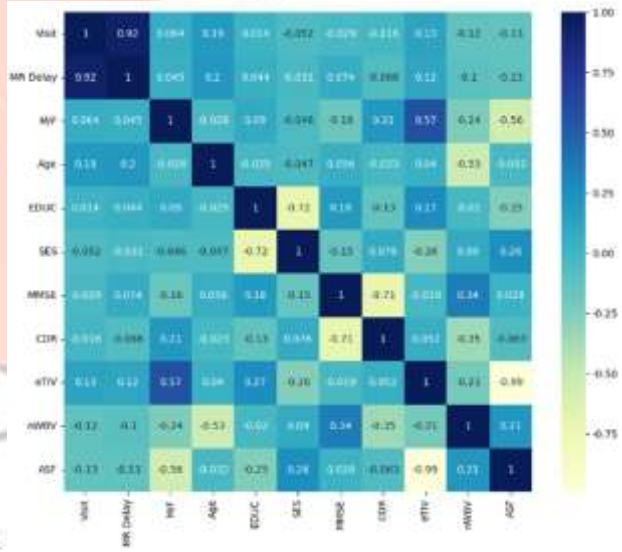

Figure 2

structure and the second dimensionless number ($Ca.Eu^{0.5}$, Ca denotes Capillary number and Eu is Euler number) governs hydrodynamics of liquid in these structures. Using the trained model for the testing dataset indicates an excellent performance of the AI model in prediction of heat flux as a function of independent variables. Furthermore, the ML-model is assessed for two cases of experimental data of two independent research groups and showed a high prediction accuracy.

GOVERNING PARAMETERS AND DATASET Thin film evaporation in hierarchical structures in three geometrical forms is shown in Fig. 2. Case (a) represents a nanomembrane assembled on top of a micro-pillared structures; case (b) shows an inverse opal structure decorated with nanopores on the surfaces of opal cavities; case (c) highlights micro-pillared structure decorated with nano particles on the external surface of these pillars. In the hierarchical structures, under steady-state condition, the working fluid is supplied to the structure to compensate for the liquid loss via evaporation. When the hydrodynamic pressure loss in the structure exceeds the fluid driving forces, the heated structure dries out due to liquid

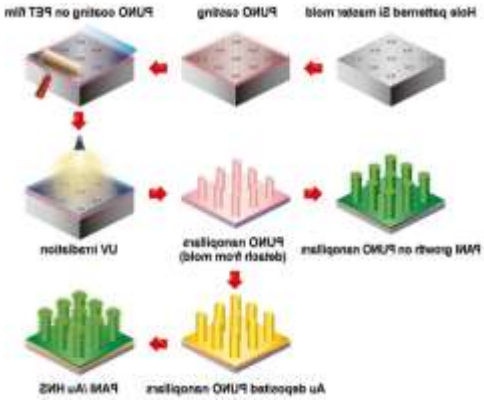

Figure 3

starvation. In design of hierarchical structures, to minimize the pressure losses, the fluid flow regime is divided into two length scales;

(1) A long length of fluid flow occurs in sections with small hydraulic resistance and

(2) A short length of fluid flow occurs in sections with high hydraulic resistance.

That is, the geometry of these structures could be characterized with four length scales as shown in Fig. 1. D_1 and L_1 represent hydraulic diameter and length of fluid flow in regime 1, respectively and D_2 and L_2 represent hydraulic diameter and length of fluid flow in regime 2, respectively. Note that for structures with several degree of branching, the same principle applies. The heat flux in the hierarchical structures is a function of saturation temperature of the working fluid (T_s), heat capacity of the working fluid (C_p) enthalpy of phase change (h_{fg}) and temperature of the hierarchical structure (T_w). These thermodynamic properties could be summarized in dimensionless Jacob number (Ja) as written below. The driving force for liquid flow in these structures could be capillary force or/and an external pumping force, while the opposing force for fluid flow is the viscous forces. Momentum conservation by these forces governs fluid velocity in these structures and may be denoted by dimensionless number of $Ca.Eu^{0.5}$ as defined

$$Ja = \frac{Cp(T_w - T_{sat})}{h_{fg}} \quad (1)$$

$$Ca = \frac{\mu U}{\gamma} \quad (2)$$

$$Eu = \frac{\Delta p}{\rho U^2} \quad (3)$$

Where μ [Pa.s] is the viscosity of the working fluid, U [ms^{-1}] is the mean velocity of the flow, γ [Nm^{-1}] is the surface tension of the fluid, Δp [Pa] is the driving force in the hierarchical structure, which is the summation of capillary pressure and external pressure and ρ [kgm^{-3}] is the density of the fluid. Through a comprehensive study of literature on thin film evaporation, 2500 experimental data were collected of heat flux in various hierarchical structures for different working fluids. The collected data set is included in Supplementary Information, S1.Geometrical features is determined of these hierarchal structures (D_1, L_1, D_2, L_2) and governing dimensionless numbers. Note that the data set includes various types of working fluids (i.e. water, isopropanol, pentane, methanol, ethanol, R245fa and FC-72). It should be added that in thin film evaporation, density of contact line (α), which is defined as a fraction of wetted perimeter in the hierarchal structure over the total area is another governing factor. However, due to sparse distribution and

Figure 4

large scattering of data in the literature on this variable, we did not include this feature in the AI platform as it leads to a decrease in the accuracy of the prediction. Table 1 shows the range of all of the extracted variables determining heat flux with their distribution for the training of the AI-model. The details of all experimental data sets used for the proposed AI model are summarized in Supplementary Information S1 and Table S1. 6 Table 1.

Table 1. Input parameters and their ranges in the collected dataset.			
	D_1 (μm)	L_1 (μm)	D_2 (μm)
Range	0-7042	0-20000	0.056-662.000
	L_2 (μm)	Ja	$Ca.Eu^{0.5}$
Range	0.2-900.	0.00031-0.89900	0.0021-3.030

METHODOLOGY FLOWCHART A flowchart illustrating the analysis sequence of data set and AI training and testing is shown in Fig. 5. As reported in the previous part, six governing variables (D_1, L_1, D_2, L_2, Ja, $Ca.Eu^{0.5}$) were chosen as input parameters to develop th

AI model. The data set contains 2500 experimental samples, covering a wide range of heat flux values and collected from various reports in the literature. Among this data set, 85% of the total data (2000 samples) were randomly used for training, and the remaining 15% of the data (550 samples) were used for the testing. Before training, the input and output parameters were normalized into a range between zero and one to improve the accuracy and convergence speed of the developed AI. For the data regression, we employed the RF algorithm implemented in scikitlearn, a reliable, flexible, and fast algorithm that requires minimal hyperparameter tuning. The RF algorithm is an ensemble learning method that operates by constructing several randomized decision trees at training time and outputting the trees' average predictions. The Out Of Bag (OOB) error which measures the prediction error of Figure 5

a random forest model, converged to its minimum value when we set the number of trees equal to 1000 hence, in this work, the number of trees in the forest was set 1000. After training the train set with the RF model, several statistical metrics are used to assess the accuracy and performance of the model on the test set, which include the correlation coefficient (R^2), mean absolute percentage of error (MAPE) and root mean squared error 7 (RMSE). The definition of these statistical metrics is given in the Supplementary Information, S2. Once validated, we assessed performance of the AI model by predicting heat flux of two forms of hierarchical structures reported by independent research groups, and there is excellent agreement between AI model predictions and reported experimental data.

RESULTS AND DISCUSSION The proper selection of independent variables in the AI model plays an important role in accuracy of the model. Figure 6 shows the importance of each input parameter on prediction of the heat flux. To measure importance of each input parameter in a RF model after training, the values of that specific input are rearranged among the training data, and prediction error is again computed on this perturbed dataset. The importance score of that specific input parameter is calculated by averaging the difference in prediction errors before and after the rearrangement. In the end, the score is normalized by the standard deviation of these differences. Features that produce large values for this score are more important than features that have small values. As discussed earlier, we classified all six independent variables into three separate categories; geometry, heat transfer and hydrodynamics. As indicated in Fig. 6, Ja plays the most important role in predictions of AI model and Ca.Eu0.5 comes in the second place. This is an expected outcome as there is a direct correlation between heat flux and Figure 6

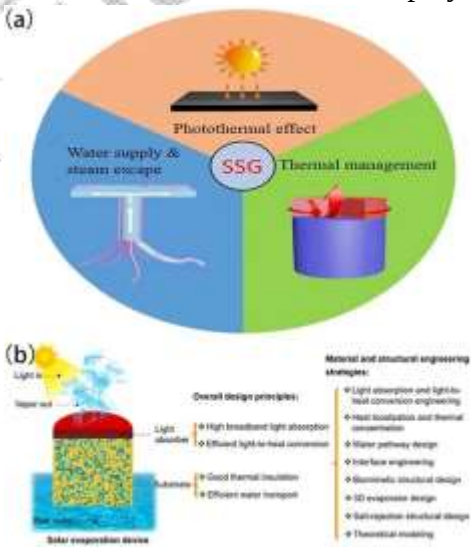

Ja number in most of the reported studies. The second important category is hydrodynamics (i.e. $Ca.Eu^{0.5}$), where the driving force, viscous losses and hydrodynamic properties of the working liquid affect heat flux. The last category is geometry of the hierarchical structures. In this category, L_2, the length of fluid flow in predefined regime 2, plays the dominant role in predicting heat flux values. That is, the length of 8 fluid flow in smaller length scale (i.e. nanoscale) is the critical factor to tune heat flux in the hierarchical structures. Once developed, in the first step, we compared predictions of AI model with the train set as shown in Fig. 7a. After, we compared the predictions with the test set (i.e. 20% of the data) as shown in Fig. 7b. As shown, there is a good agreement between the predicted values by AI model and both data sets. In order to investigate linearity between the train or test sets and experimental measurements, we also calculated Pearson correlation. A Pearson correlation coefficient value close to 1, means the relationship between the train or test sets and experimental measurements is exactly linear. We calculated the Person values of 0.9912 and 0.9901 for training and test sets respectively. We should add that the experimental measurements of heat flux have inherent error in metrologies that could vary between various groups. This error could contribute to some degree of error in AI predictions.

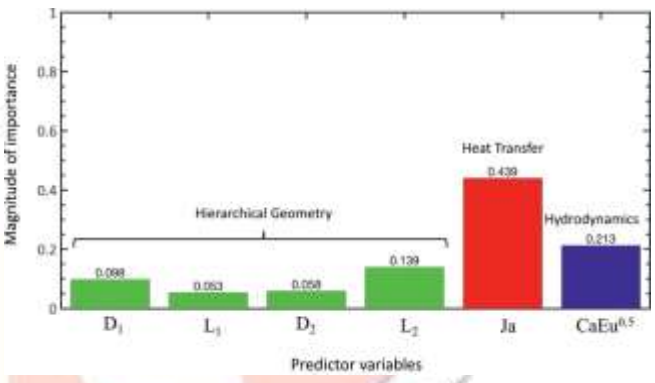

Figure 7

The relative error in the AI prediction of heat flux were demonstrated against experimental data to further validate the performance of the model for the training and testing phases in Supplementary Information S3 and Fig. S1. To further assess the performance of the developed AI model various statistical metrics were thoroughly implemented. These statistical criteria for comparing the AI model's training and testing phases are summarized in Table 2.

Table 2 Performance of the AI predictive model for the training and testing sets using various statistical criteria

	R^2	RMSE	MAPE
Train set	0.978	26.3	16.7%
Train set	0.978	28.5	17.4%

AI models usually include a predetermined degree of randomness in their training methods and this comes with a detrimental effect on the generalization and stability of the model83. In the 9 training process, the model is updated using a randomized procedure that will result in model's final predictions every time the training code is executed. The only way to ensure that the results of different trained models are reproducible is to set a quantity known as the random seed, which controls how random procedures are generated.84 This number is a starting point for the sequence, and the guarantee is that if you start from the same seed number, the trained model will predict completely similar values. To examine stability and generalization of our AI algorithm, we executed the training code with three random initial conditions and compared predictions of the AI models on thin film evaporation in a nanomembrane. The three different initial conditions are induced by defining different seed numbers of 10, 20, and 30. The schematic of the examined

structure for thin film evaporation is shown in Fig. 8. Water, chosen as the working fluid, was driven by capillary pressure across an anodic aluminum oxide (AAO) membrane Figure 8 with a nominal pore size of 50 nm and thickness of 100 µm. The evaporation occurs on the membrane's heated surface, and the resulting vapor molecules carry the heat from the solid surface to the vapor space. In this experiment, the input parameters are D_1 = 4.6 mm, L_1 = 1.6 cm, D_2 = 50 nm, L_2 = 100 µm, $Ca.Eu^{0.5}D.F$ = 0.053 and the Ja number varies between the wide range of 0 to 0.135. The predicted values of heat flux by the AI model as a function indicates, for all different random initial conditions, the AI models display completely similar output patterns, which is a proof for the stability and generalization of the RF algorithm used on the training data set. This analysis reveals that the AI model predictions are independent of the random initial conditions in the training process. In the next step and to further assess the AI model, we examined the model's predictions with two independent studies on thin film evaporation in hierarchical structures conducted by 10 different research groups. The different metrological instrumentation by independent groups leads to some degree of error in the reported values. Figure 9 represents the schematic of the hierarchical structure examined by Hanks et al.58. The Figure 9 membrane (shown in grey) was bonded to a high permeability silicon micro-channel array (shown in red) to create a hierarchical structure, to achieves high capillary driving force with enhanced permeability. The working fluid (Pentane) wicks into the liquid supply channels (shown in red) before flowing through the membrane pores and evaporating at the membrane surface. The backside of this hierarchical structure is attached to a heater to induce the heat flux and resistive temperature sensors to measure the structure's temperature. The nanoporous membrane 600 nm thick with 110 nm pores is suspended over a liquid supply network of microchannels that are 200 µm of different Ja number is plotted in Fig. 9 for three independent initial conditions. As this figure indicates, for all different random initial conditions, the AI models display completely similar output patterns, which is a proof for the stability and generalization of the RF algorithm used on the training data set. This analysis reveals that the AI model predictions are independent of the random initial conditions in the training process. In the next step and to further assess the AI model, we examined the model's predictions with two independent studies on thin film evaporation in hierarchical structures conducted by 10 different research groups. The different metrological instrumentation by independent groups leads to some degree of error in the reported values. The nanoporous membrane 600 nm thick with 110 nm pores is suspended over a liquid supply network of microchannels that are 200 µm long, 2µm wide, and 2 µm high. As we defined earlier, in all the hierarchical structures, the fluid flow is divided into two regimes, (1) a long length of fluid flow occurs in sections with small hydraulic resistance, which is microchannels in this case, and (2) a short length of fluid flow occurs in sections with high hydraulic resistance, which is the nanoporous membrane in this study. Hence, for this study, the Figure 10

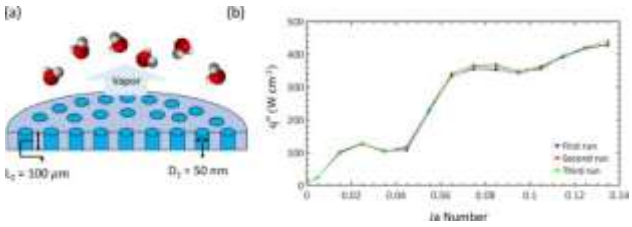

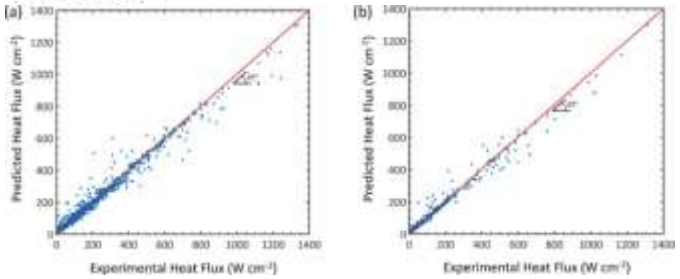

geometrical input parameters are: D_1 = 2 µm (i.e. hydraulic diameter of microchannels), L_1 = 100 µm (i.e. the average distance that liquid pass to reach the membrane which is equal to half of the microchannels' length), D_2 =110 nm (i.e. pores' diameter) and L_2 = 600 n(i.e. membrane's thickness). The $Ca.Eu^{0.5}D.F$ number is calculated as 0.4686 for this study based on the capillary driving force and the hydrodynamic properties of the working fluid. We deliberately excluded this work's data from the data sets. Having all the input parameters for this study, we compared prediction of AI model with the measured values as a function of Ja number shown in Fig. 10. The dashed lines envelop the uncertainty associated with the measurements.

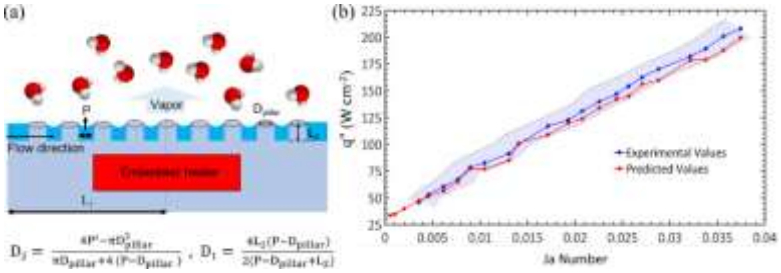

Figure 11

As shown, there is a good agreement between the measured experimental values and the predicted ones by the AI 11 model. This suggests that the AI model could be used for prediction of heat flux in hierarchical structure minimizing the cost and time challenges of experimental counterpart. For the second independent case study, we chose the experimental study conducted by Bigham et al.55. As depicted in Fig. 7a, this experimental study is conducted on a microchannel that is 8 mm long, 300 µm wide, and 175 µm tall. Along the flow direction, the bottom wall of the microchannel has pillars with diameter of 10 µm (i.e. D_{pillar} = 10 µm), a height of 20 µm (i.e. L_2 = 20 µm), and an edge-to-edge spacing of 30 µm (i.e. P = 30 µm). There is an embedded heater inside this structure to generate the required heat flux during the experiments. The evaporation occurs between the pillars, and the resulting vapor molecules carry the heat from the structure to the vapor space. The predefined regime 1 occurs in the microchannel for this case, and the predefined regime 2 occurs in the void space between pillars. Hence, for this study the geometrical input parameters are : D1 = 24 µm (i.e. hydraulic diameter along the flow direction inside the microchannel, calculated by equation (4), L^1 = 4 mm (i.e. average distance that liquid pass to reach the evaporative interface which is equal to half of the microchannels' length.) , D2 = 40.2 µm (i.e. hydraulic diameter along the pillars, calculated by equation (5), L2 = 20 µm (i.e. pillars' length). The $Ca.Eu^{0.5}D.F$ number is calculated for this study, and it has a value of 0.0143.

$$D_1 = 4L_2(P - D_{pillar})/(2(P - D_{pillar} + L_2) \quad (4)$$

$$D_2 = 4P^2 - \pi D_{pillar}^2 /(\pi D_{pillar} + 4(P - D_{piller}) \quad (5)$$

Having all the input parameters for this study, we ran the AI model to predict heat flux in this structure as a function of Ja number. Figure 7b depicts the comparison between the predicted heat flux curve as a function of Ja number with the measured ones. The area between dashed lines illustrates the errors in the measurements. Although, in this experimental set, the minimum 12 reported value of Ja was 0.003, we included the predictions for lower Ja numbers. As shown, there is a decent agreement between the measured experimental values and the predicted values. This is remarkable as the trained model explains all the experimental findings from another independent group with high accuracy.

CONCLUSIONS In summary, we cast a methodology and a predictive AI platform for thin film evaporation in hierarchical structures. Through physics of thin film evaporation, we determined six independent variables that govern heat flux in hierarchical structures. Four of these variables are function of geometry of the hierarchical structure, one governs heat transfer in the structure and the last one determines the hydrodynamics of flow in these structures. A complete data set on thin film evaporation in hierarchical structures was collected from various independent research groups. The AI model was developed based on the random forest algorithm, a reliable algorithm with minimal hyperparameter tuning. The developed AI model shows a good agreement with both the train and test sets with statistical metrics of (R^2 = 0.99, RMSE=29.6, MAPE= 18.1%) for the test set. Based on the analysis of the AI model, the length scale of the smaller length scale of the hierarchical structure (i.e. nanoscale) is the most ruling dimension for design of hierarchical structures for maximum heat

dissipation. The stability and generalization of AI model predictions is shown on an AAO membrane for three independent initial conditions. The AI model was further assessed through prediction of heat flux as a function of Ja for two independent studies from different research groups. The good agreement between AI predictions and measurements further confirm the accuracy of the developed methodology and AI model. We should emphasize that the develop general AI model could be implemented for various form of working fluids. This work provides a foundation and rational methodology to use data science 13 to guide future development of hierarchical structures for thermal management of a wide spectrum of system including photonics/electronics, hypersonic aviation and energy/water systems.

REFERENCES

(1) Zhang, T. J.; Peles, Y.; Wen, J. T.; Tong, T.; Chang, J. Y.; Prasher, R.; Jensen, M. K. Analysis and Active Control of Pressure-Drop Flow Instabilities in Boiling Microchannel Systems. Int. J. Heat Mass Transf. 2010, 53 (11–12), 2347–2360.

(2) Gao, Q.; Li, H.; Zhang, J.; Xie, Z.; Zhang, J.; Wang, L. Microchannel Structural Design For a Room-Temperature Liquid Metal Based Super-Stretchable Sensor. Sci. Rep. 2019, 9 (1), 1–8.

(3) Koukoravas, T. P.; Ghosh, A.; Mahapatra, P. S.; Ganguly, R.; Megaridis, C. M. SpatiallySelective Cooling by Liquid Jet Impinging Orthogonally on a Wettability-Patterned Surface. Int. J. Heat Mass Transf. 2016, 95 (2016), 142–152.

(4) Wayner, P. C.; Kao, Y. K.; LaCroix, L. V. The Interline Heat-Transfer Coefficient of an Evaporating Wetting Film. Int. J. Heat Mass Transf. 1976, 19 (5), 487–492.

(5) Wang, H.; Garimella, S. V.; Murthy, J. Y. An Analytical Solution for the Total Heat Transfer in the Thin-Film Region of an Evaporating Meniscus. Int. J. Heat Mass Transf. 2008, 51 (25–26), 6317–6322.

(6) Plawsky, J. L.; Fedorov, A. G.; Garimella, S. V.; Ma, H. B.; Maroo, S. C.; Chen, L.; Nam, Y. Nano-and Microstructures for Thin-Film Evaporation-A Review. Nanoscale Microscale Thermophys. Eng. 2014, 18 (3), 251–269. 15

(7) Ma, H. B.; Cheng, P.; Borgmeyer, B.; Wang, Y. X. Fluid Flow and Heat Transfer in the Evaporating Thin Film Region. Microfluid. Nanofluidics 2008, 4 (3), 237–243.

(8) Wang, X.; Li, Y.; Malen, J. A.; McGaughey, A. J. H. Assessing the Impact of Disjoining Pressure on Thin-Film Evaporation with Atomistic Simulation and Kinetic Theory. Appl. Phys. Lett. 2020, 116 (21), 213701.

(9) Liu, R.; Liu, Z. Study of Boiling Heat Transfer on Concave Hemispherical Nanostructure Surface with MD Simulation. Int. J. Heat Mass Transf. 2019, 143, 118534.

(10) Xiao, R.; Enright, R.; Wang, E. N. Prediction and Optimization of Liquid Propagation in Micropillar Arrays. Langmuir 2010, 26 (19), 15070–15075.

(11) Farokhnia, N.; Sajadi, S. M.; Irajizad, P.; Ghasemi, H. Decoupled Hierarchical Structures for Suppression of Leidenfrost Phenomenon. Langmuir 2017, 33 (10), 2541–2550.

(12) Gu, Z.; Kothary, P.; Sun, C. H.; Gari, A.; Zhang, Y.; Taylor, C.; Jiang, P. EvaporationInduced Hierarchical Assembly of Rigid Silicon Nanopillars Fabricated by a Scalable Two-Level Colloidal Lithography Approach. ACS Appl. Mater. Interfaces 2019, 11 (43), 16 40461–40469.

(13) Sharratt, S.; Cha, G. Characterization and Modeling of the Heat Transfer Performance of Nanostructured Cu Micropost Wicks. J. Heat Transfer 2011, 133 (10).

(14) Min, D. H.; Hwang, G. S.; Kaviany, M. Multi-Artery , Heat Pipe Spreader. Int. J. Heat Mass Transf. 2009, 52 (3–4), 629–635.

(15) Weibel, J. A.; Garimella, S. V; North, M. T. Characterization of Evaporation and Boiling from Sintered Powder Wicks Fed by Capillary Action. Int. J. Heat Mass Transf. 2010, 53 (19–20), 4204–4215.

(16) Brown, K. A.; Brittman, S.; Maccaferri, N.; Jariwala, D.; Celano, U. Machine Learning in Nanoscience: Big Data at Small Scales. Nano Lett. 2020, 20 (1), 2–10.

(17) Bassman, L.; Rajak, P.; Kalia, R. K.; Nakano, A.; Sha, F.; Sun, J.; Singh, D. J.; Aykol, M.; Huck, P.; Persson, K.; et al. Active Learning for Accelerated Design of Layered Materials. npj Comput. Mater. 2018, 4 (1), 1–9.

(18) Lazarovits, J.; Sindhwani, S.; Tavares, A. J.; Zhang, Y.; Song, F.; Audet, J.; Krieger, J. R.; Syed, A. M.; Stordy, B.; Chan, W. C. W. Supervised Learning and Mass Spectrometry 17 Predicts the in Vivo Fate of Nanomaterials. ACS Nano 2019, 13 (7), 8023–8034.

(19) Ma, W.; Cheng, F.; Liu, Y. Deep-Learning-Enabled On-Demand Design of Chiral Metamaterials. ACS Nano 2018, 12 (6), 6326–6334.

(20) Frey, N. C.; Wang, J.; Vega Bellido, G. I.; Anasori, B.; Gogotsi, Y.; Shenoy, V. B. Prediction of Synthesis of 2D Metal Carbides and Nitrides (MXenes) and Their Precursors with Positive and Unlabeled Machine Learning. ACS Nano 2019, 13 (3), 3031–3041.